Scientific Research Publishing

Open Journal of Applied Sciences, 2025, 15(12), 4043-4058
https://www.scirp.org/journal/ojapps
ISSN Online: 2165-3925
ISSN Print: 2165-3917

Comparison of Wheel/Rail Friction Temperature under Traction and Braking Condition

Zewang Yuan

College of Locomotive and Rolling Stock, Guangzhou Railway Polytechnic, Guangzhou, China
Email: yzw0746@163.com

How to cite this paper: Yuan, Z.W. (2025) Comparison of Wheel/Rail Friction Temperature under Traction and Braking Condition. *Open Journal of Applied Sciences*, **15**, 4043-4058.
https://doi.org/10.4236/ojapps.2025.1512261

Received: November 20, 2025
Accepted: December 19, 2025
Published: December 22, 2025

Copyright © 2025 by author(s) and Scientific Research Publishing Inc.
This work is licensed under the Creative Commons Attribution International License (CC BY 4.0).
http://creativecommons.org/licenses/by/4.0/

Open Access

Abstract

The purpose of this paper is to compare the differences in wheel/rail friction temperature under traction and braking, for further analysis of the distinction of adhesion performance under traction and braking. A three-dimensional (3D) finite element (FE) model was developed, and the wheel/rail temperatures under different slippages and speeds were calculated. The results show that the wheel under braking gets the highest temperature, followed by the rail, and the wheel under traction gets the lowest temperature. When the slippage is less than 20%, the differences of the peak temperatures of the wheel under baking and traction are within 101.68˚C. After exceeding 20%, the difference increases sharply. The difference is not sensitive to the vehicle speed, which keeps about 100˚C when the speed is over 50 km/h. With the increasing slippage, the temperature differences between the leading and trailing edge under traction are decreasing, while those under braking are increasing. Under the extreme condition of the wheel sliding, the wheel temperature is concentrated on the contact patch. The proposed FE model gives a method to simulate wheel/rail contact temperature under various conditions. There is a big difference in the temperature under traction and braking, which helps to understand the distinction of the adhesion performance under traction and braking.

Keywords

Wheel/Rail Contact, Friction Heat, Traction, Braking, Moving Heat Source

1. Introduction

The wheel/rail slip produces the tangential force, namely, creep forces, which accelerate and brake the vehicle [1]. At the same time as the traction or braking, the

local temperature on the contact region rises rapidly due to the frictional work. On the one hand, the friction heat affects the properties of the material near the contact area, such as softening [2]-[4], reduction of elastic modulus and strength [2] [5]. On the other hand, the friction heat transforms the oxidation film of the wheel/rail interface [6]-[8].

It is a widely accepted fact that the wheel/rail coefficient of friction (COF) decreases with increasing sliding speed in dry friction [9]-[11]. A higher speed means a larger heat generation, which changes the state of the wheel/rail friction system. The quantity of heat relates to the usage of the wheel/rail adhesion, which determines the performance of the traction and braking. The distance the wheel rolls on the rail is different per unit time in traction and braking [12]. This means there is a difference in the friction work between the two running conditions.

Since it is difficult to measure the wheel/rail temperature during the operation, theoretical calculation and numerical simulation were adopted. Analytical method [13]-[15] and two-dimensional finite element method (FEM) [16] [17] were the main methods used in the early stage. In recent years, 3-D FEM [18]-[22] has been adopted widely for calculating wheel/rail contact temperature. According to the loading method of the heat flow, the FEM are divided into the thermal-mechanical coupling [18] [19] and the moving heat source method [21] [22]. The thermal-mechanical coupling method has high requirements for the mesh size and time step; it is not realistic for a long-time simulation. In the moving heat source method, the wheel/rail friction heat was equivalent to a heat source moving along the rail to simulate the rail temperatures under rolling plus sliding conditions [18] [19]. Currently, the heat source method cannot realize a heat source that rotates around on the tread, which limits the investigation of wheel temperature under the rolling plus sliding condition.

Based on the software MSC. Marc, a Fortran subroutine was developed to realize a heat source that moves along the rail and rotates around on the tread in this paper. To reflect the real contact patch, an elliptic cylinder heat source was used. The wheel/rail temperatures under traction and braking were calculated and compared, and the effects of slippage and speed on the temperature field were analyzed.

2. Moving Heat Source

Wheel/rail friction heat is generated from the friction work on the contact patch. According to Coulomb's friction law, the tangential stress p_τ can be calculated by the following Equation.

$$p_\tau(x,y) = \mu \cdot p(x,y) \tag{1}$$

where μ is the coefficient of friction (COF).

When the vehicle drives on the rail with a speed v, and the wheel rotates with an angular speed w, the relative sliding speed v_s can be expressed as follows:

$$v_s = \omega r_w - v \tag{2}$$

$$v_s = v \cdot s \tag{3}$$

where r_w is the wheel radius, s is the slippage, which is defined as the ratio of the difference between the wheel speed and vehicle speed to the vehicle speed, and it is positive in traction and negative in braking.

The total heat flux on the contact patch can be calculated by Equation (4). According to the principle of energy equivalence, the semi-ellipsoid heat flux $q(x,y)$ can be replaced by an average heat flux $\overline{q}$, as seen in **Figure 1**, and the relationship between $\overline{q}$ and $q(x,y)$ is described by Equation (5). Substituting from Equation (4) to Equation (5), the expression for $\overline{q}$ is obtained as seen in Equation (6). Since the area of the contact patch is very small, and is generally about 100 mm^2 [23], the equivalent method has little effect on the temperature field of the wheel and rail surface.

$$q(x,y) = \mu \cdot v_s \cdot p(x,y) \tag{4}$$

$$\iint_S q(x,y)\mathrm{d}x\mathrm{d}y = \iint_S \overline{q}\mathrm{d}x\mathrm{d}y \tag{5}$$

$$\overline{q} = \mu \cdot v_s \cdot \overline{p} = \frac{\mu \cdot v_s \cdot P}{\pi ab} \tag{6}$$

where S is the contact surface, $\overline{q}$ is the average heat flux, $\overline{p}$ is the average contact pressure, P is the wheel load，a and b are the longitudinal and lateral semi-axis length of the contact patch, respectively.

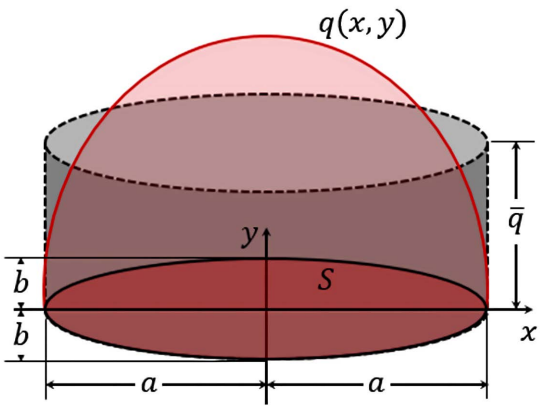

Figure 1. The heat flux distribution on the contact patch and its equivalent treatment.

The total heat generation equals the heat absorbed by the wheel and rail, then the expressions of heat flux for the wheel and rail are seen in Equations (7) and (8), respectively.

$$q_w = \gamma \mu v_s \overline{p} \tag{7}$$

$$q_r = (1-\gamma)\mu v_s \overline{p} \tag{8}$$

where q_w and q_r are the heat flux into the wheel and rail, respectively, γ is the heat portion. According to Limpert [24], the expression for γ is as follows:

$$\gamma = \frac{\sqrt{\rho_r c_r \lambda_r}}{\sqrt{\rho_r c_r \lambda_r} + \sqrt{\rho_w c_w \lambda_w}} \tag{9}$$

where ρ_w, ρ_r, c_w, c_r, λ_w, λ_r are the density, specific heat, and thermal conductivity of the wheel and rail, respectively.

Figure 2(a) is the schematic of the heat source rotating around on the tread, and the plan in Figure 2(c) is expanded from the part $AA'B'B$ of the tread as seen in Figure 2(a). A Cartesian coordinate system $yo'u$ is established with the y-axis and u-axis, where the u-axis is on the line of the elliptic centers and perpendicular to the y-axis. In the case of no transversal displacement of the wheelset, the coordinates of the loading nodes will not be changed in the direction of the y-axis, and are within the range of $y = \pm b$. Over a period of t_i, the origin (the center of the ellipse) transferred from O_0 to O_i, with a distance of d_w, which corresponds to the coordinates of u in Figure 2(c). Figure 2(b) is the projection of the tread part $AA'B'B$ on the y-axis. According to the geometry relationship in Figure 2(b), the expression of d_w is given as follows:

$$d_w = (\omega t_i - \theta_0) r_w \tag{10}$$

where θ_0 is the initial deflection angle, for seeing the full elliptic loading region at the initial moment. According to the size of elliptic contact patches, θ_0 is chosen to be 0.025 rad.

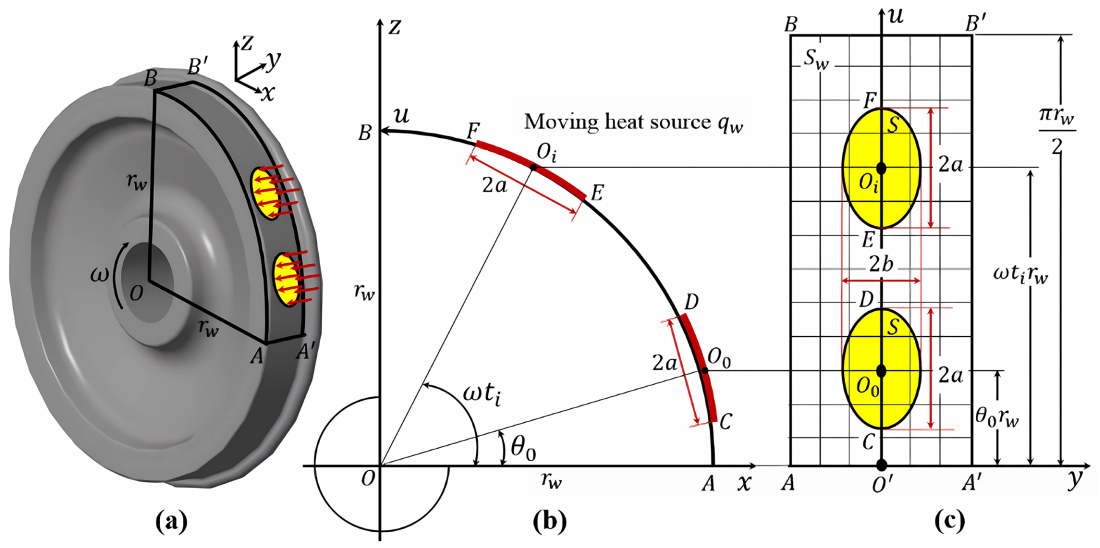

Figure 2. The heat source rotates around on the tread: (a) global view; (b) front view (first quartile of the xoz); (c) the plan expanded from the tread.

When loading nodes are located in the elliptic contact surface S as seen in Figure 2(c), the value of the heat flux will be assigned as q_w, otherwise it will be put at 0. The heat flux is given as follows:

$$q = \begin{cases} q_w & (u, y) \in S \\ 0 & (u, y) \in S_w - S \end{cases} \tag{11}$$

where S_w is the surface of the wheel, S is the elliptic contact surface, the expression for the surface S at t_i moment is given as follows:

$$S:\frac{\left(\omega t_i r_w-\theta_0 r_w\right)^2}{a^2}+\frac{y^2}{b^2}\le 1 \tag{12}$$

Figure 3(a) is the schematic of the heat source moving along the x-axis on the rail with speed v. Figure 3(b) is the schematic of the relative position of the elliptic heat flux on the plan $xo'y$ between the initial moment and t_i moment. In the case of no transversal displacement of the wheelset, the coordinates of the loading nodes will not be changed in the direction of the y-axis, and will remain within the range of $y=\pm b$. Over a period of t_i, the origin (the center of the ellipse) transferred from O_0 to O_i, with a distance of d_r, whose expression is given by Equation (23):

$$d_r=vt_i-l_0 \tag{13}$$

where l_0 is the initial offset distance, for seeing the full elliptic loading region at the initial moment. According to the size of the elliptic contact patches, l_0 is chosen to be 15 mm.

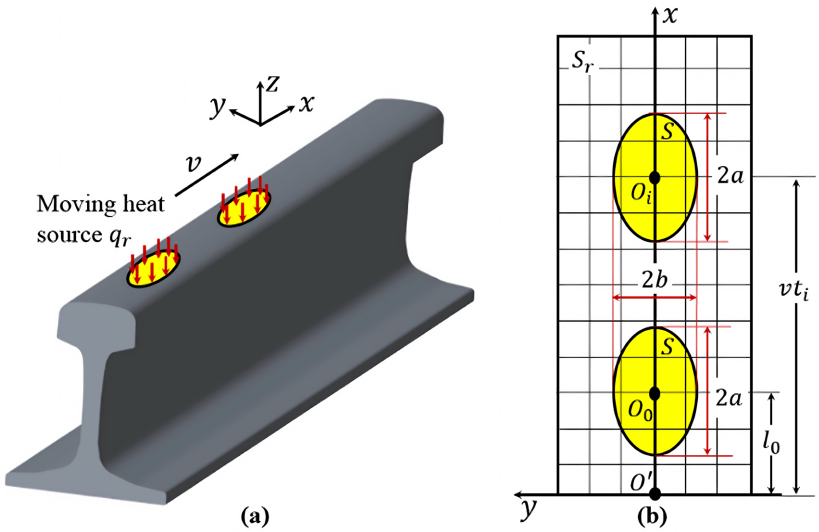

Figure 3. Heat source moving along the rail: (a) global view; (b) top face of the rail.

When loading nodes are located in the elliptic contact surface S, as seen in Figure 3(b), the value of the heat flux will be assigned as q_r, otherwise it will be set at 0. The heat flux is given as follows:

$$q=\begin{cases}q_r & (x,y)\in S\\ 0 & (x,y)\in S_r-S\end{cases} \tag{14}$$

where S_r is the surface of the rail, S is the elliptic contact surface, the expression of the surface S at t_i moment is given as follows:

$$S:\frac{\left(x-vt_i+l_0\right)^2}{a^2}+\frac{y^2}{b^2}\le 1 \tag{15}$$

3. FE Model

To ensure the accuracy of the calculation, the mesh size near the contact region

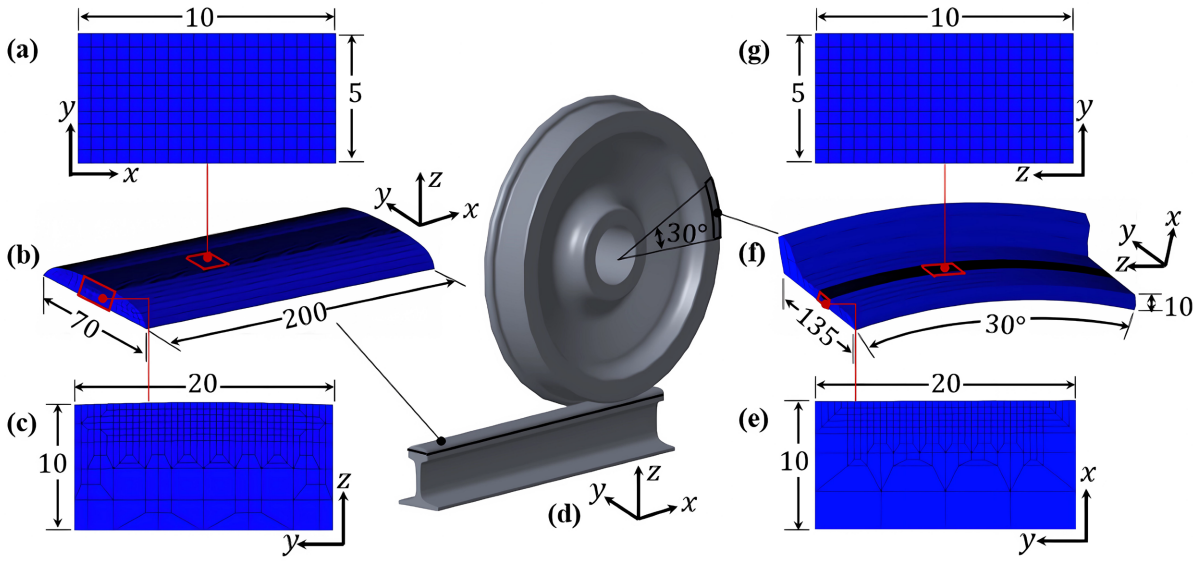

Figure 4. Wheel/rail FE model: (a) mesh size of the rail contact area; (b) FE model of the rail; (c) cross section of the rail; (d) wheel/rail 3-D model; (e) cross section of the wheel; (f) FE model of the wheel; (g) mesh size of the wheel contact area.

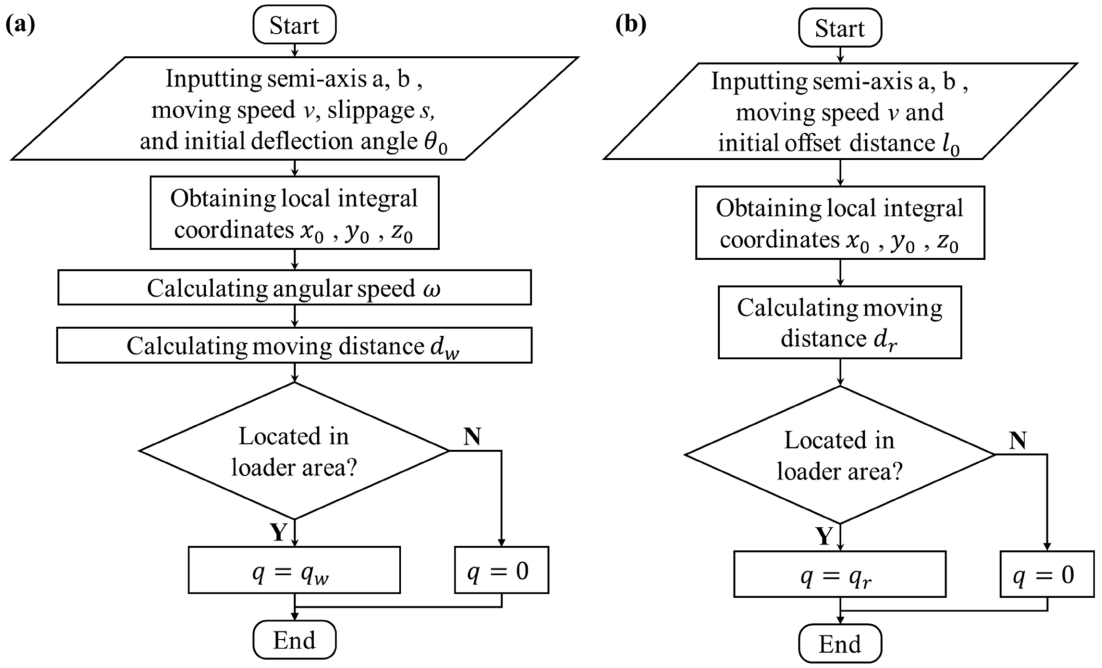

Figure 5. Flowchart of the Fortran subroutine (a) wheel and (b) rail.

should be small as soon as possible. However, considering the limitations of the computing resources and time, the total number of elements cannot be too large. To balance the contradiction, a part of the wheel and rail, which are greatly affected by heat flow, were taken out to establish a FE model, respectively. The length of the rail is 200 mm, and the angle of the wheel is 30˚, as seen in Figure 4(d) and Figure 4(f). Since the depth affected by friction heat is within 2 mm [17], the modeling dimension of the wheel and rail in the depth direction was taken to be 10 mm,

respectively, as seen in Figure 4(c) and Figure 4(e). The dimension of the mesh refinement in the width direction is 20 mm, as seen in Figure 4(c) and Figure 4(e), which fully took the lateral-axis length of the contact patch into consideration. The refined mesh size near the contact patch is 0.5 × 0.5 mm^2. In the 3-D model, the type of wheel tread is LMA, and the rail is CHN60. The FE model with element type HEX8 was established by MSC. Marc, and a Fortran subroutine was used to realize the moving of the heat source, as shown in Figure 5. The wheel model contains 120,120 elements and 135,828 nodes, and the rail model contains 140,800 elements and 156,390 nodes.

3.1. Boundary Conditions

The rail is in a state of natural convection, so the film coefficient can be chosen as 10 W/(m^2·˚C) by referring to Ertz *et al.* [15]. While the wheel is in a state of forced convection. According to the empirical expression given by Bergman *et al.* [25], the film coefficients of the wheel under different speeds are calculated as seen in Table 1. The ambient temperature T_A was assumed to be 25˚C.

Table 1. Film coefficient of the wheel and rail.

Speed, v (km/h)	20	50	100	200	300
h_w (W/m^2·˚C)	15	28	45	73	97
h_r (W/m^2·˚C)	10	10	10	10	10

3.2. Simulated Parameters

Since the material properties will be changed due to the temperature rise, wheel/rail material parameters vary with temperature are chosen for the calculation from Chen and Lee [5], and are shown in Table 2.

Table 2. Temperature-dependent mechanical and thermal properties.

Temperature, T (˚C)	Young's Modulus, E (GPa)	Poisson's Ratio, v	Mass Density, ρ (kg/m^3)	Conductivity, λ (W/m˚C)	Specific Heat, c (J/kg˚C)	Thermal Expansion, α (ppm/˚C)
25	209	0.30	7850	47.7	490.1	11.0
100	207	0.30	7850	48.9	499.9	11.6
650	105	0.36	7850	57.8	571.1	14.8
1000	50	0.39	7850	63.4	617.1	15.7
1450	2.1	0.40	7850	76.4	671.8	16.1

As the material composition of the wheel and rail is essentially identical, both being high-carbon steel, the parameters listed in Table 2 were employed throughout the modelling and calculation processes. The values of the relevant material parameter at room temperature were chosen for calculating the heat portion γ, and the calculated γ is 0.5. The simulation conditions are listed in Table 3.

Table 3. Simulation conditions.

Conditions	Wheel load, P (kN)	Semi-Axis, a (mm)	Semi-Axis, b (mm)	Average Pressure, $\bar{p}$ (MPa)	COF, μ	Slip Ratio, s (%)	Vehicle Speed, v (km/h)
1 - 10	70	7.63	5.17	554.40	0.3	5, 10, 20, 50, 100, −5, −10, −20, −50, −100	100
11 - 14	70	7.63	5.17	554.40	0.3	20	20, 50, 200, 300
15 - 18	70	7.63	5.17	554.40	0.3	−20	20, 50, 200, 300

4. Results and Discussion

Since the velocity was assumed to be a constant in the simulation, the temperatures of the rail have no difference under traction and braking. Therefore, the results of the rail provided hereafter represent the temperatures under the traction and braking.

4.1. Model Validation

To validate the model, two simulation cases consistent with Lian *et al.* [22] and Naeimi *et al.* [19] were set up. Table 4 shows the calculated peak temperature of wheel/rail and its comparison with the references. The peak temperature of the wheel and rail are 201.87˚C and 216.90˚Cin case1, respectively, while the calculation of the rail by Lian *et al.* [22] is 227˚C, then the error of the peak temperature of the rail is 4.45%. The peak temperatures of the wheel and rail are 678.19˚C and 715.90˚C in case 2, respectively, while the calculations by Naeimi *et al.* [19] are 719.70˚C and 744.10˚C, respectively; then the errors of the peak temperature of the wheel and rail are 5.77% and 3.79%, respectively. Compared with mainstream methods, the relative errors in the calculated temperatures are less than 6% in the same cases, which can be considered evidence that the model established in this paper is valid.

Table 4. Calculated peak temperatures and the comparison with the references.

	Lian *et al.* [22]	Case 1	Naeimi *et al.* [19]	Case 2
Wheel Load, P (kN)	135	135	134	134
COF (-)	0.3	0.3	0.6	0.6
Speed, v (km/h)	115	115	140	140
Slippage, s (%)	9.43	9.43	18	18
Ambient Temperature, T_A (˚C)	30	30	25	25
Film Coefficient, h (W/m²·˚C)	10	10	0	0
Wheel, T (˚C)	-	201.87	719.70	678.19
Rail, T (˚C)	227	216.90	744.10	715.90

4.2. Distinction of the Peak Temperature

The increase in slippage widens the gap in friction work between traction and brak-

ing. Figure 6 shows the variations of the peak temperatures and the difference between the braking and traction with the slippage. The peak temperature of the rail increases linearly as the slippage increases, and the peak temperatures of the wheel under braking and traction are higher and lower than that of the rail, respectively. Under braking conditions, the peak temperature of the wheel increases with the increasing slippage, and the increasing speed increases faster and faster. After sliding 1 ms, the peak temperature of the wheel is up to 2045.88˚C, which exceeds the point of phase transformation. Nevertheless, in actual operation, when the wheel-rail temperature reaches a certain high level, it can lead to thermal wear, phase transformation, and even melting of the materials. Therefore, temperatures exceeding the phase transition points during the calculation process are only used for trend assessment. It can be expected that the calculated peak value will continue to increase as the slide continues. Under traction conditions, the peak temperature of the wheel increases with increasing slippage, but the growth rate gradually slows down. When the slippage is less than 20%, the difference of the peak temperatures of the wheel under braking and traction is within 101.68˚C. After exceeding 20%, the difference increases sharply. According to Equation (2), during braking, the heat source on the wheel tread moves at the fastest rate, followed by the rail surface, with the slowest movement occurring on the wheel tread during traction. Over the same period, the accumulation of heat differs across these three states. Consequently, the wheel tread temperature is maximum during braking, followed by the rail surface, with the lowest temperature recorded on the wheel tread during traction. The results indicate that the slippage has a significant influence on the peak temperatures in braking and traction. This means there may be a large distinction in the adhesion performance between traction and braking under different slippages.

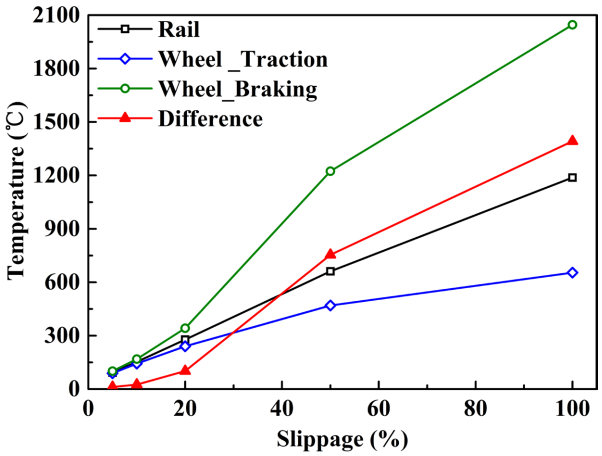

Figure 6. Peak temperatures and their differences vary with slippage.

Figure 7 shows the peak temperatures and the difference in wheel temperatures between braking and traction vary with the speed. After reaching the speed of 50 km/h, the difference remains about 100˚C. This means the difference is not sensitive to the speed.

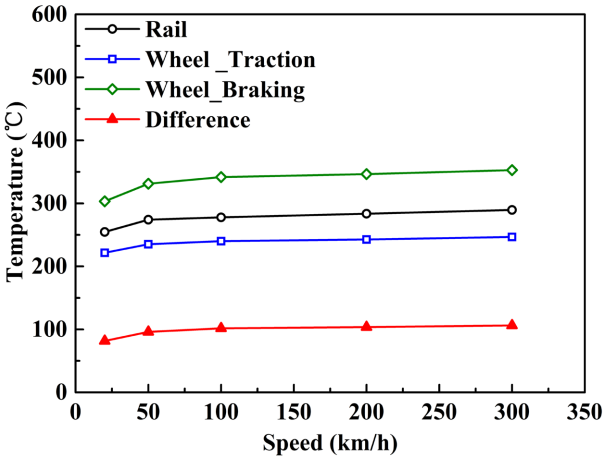

Figure 7. Peak temperatures and their differences vary with speed.

4.3. Distinction of the Temperature Variation

For the calculation of wheel/rail temperature, the major difference between the traction and braking is the speed of the heat source rotating around on the tread, which causes a distinct heat power. Figure 8 shows the temperature history curves at different slippages. The curves in the figure came from the nodes that first reached the peak temperature. It can be found that the wheel in traction is the first one to get the peak values, followed by the rail, and the wheel in braking is the last one, but the order of the reached peak temperatures is opposite.

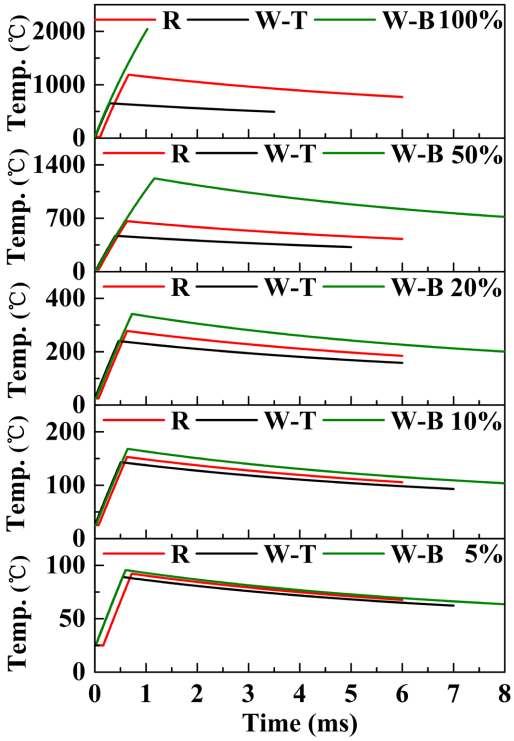

Figure 8. Temperature history curves at different slippages (R, W-T, W-B represent rail, wheel in traction, and braking, respectively).

Figure 9 shows the temperature history curves at different speeds. The curves in the figure came from the nodes that first reach the peak temperature. It can be found that the increasing rates of temperature are almost the same. However, as the speed increases, the temperatures rise faster. Since the peak values reached are different under braking and traction, the first one reached the peak value is the wheel in braking, followed by the rail, and the last one is the wheel in traction. During a short simulation period, the decreasing rates of the temperature have non-obvious differences in different running conditions. However, with increasing time, the temperature finally tends to a stable value, such as tending to 80˚C at 20 km/h.

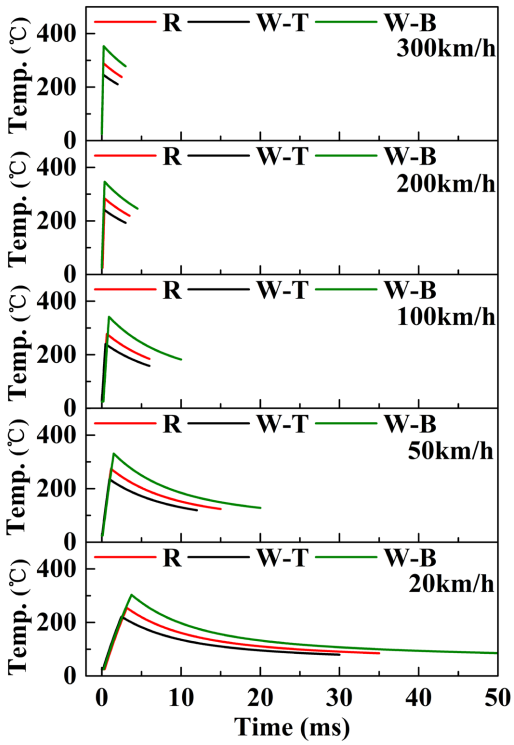

Figure 9. Temperature history curves at different speeds (R, W-T, W-B represent rail, wheel in traction, and braking, respectively).

4.4. Distinction of the Temperature Distribution

As the slippage increases, the moving speed of the heat source on the wheel in traction becomes faster, while that in braking becomes slower. Figure 10 shows the temperature contours of the surface in the rolling direction at different slippages. With the increasing slippage, the temperature contours of the rail surface are generally similar, and those of the wheel in traction are more and more uniform, but the difference between the leading and trailing edge is larger and larger in braking. Under the extreme condition of the wheel sliding, the wheel temperature is concentrated on the contact patch. Figure 11 is the temperature distribution of the nodes in the rolling direction, and the nodes are located in the line of rolling centers. As the increase of the slippage, the temperature curves in the mov-

ing ranges of the heat source are flatter and flatter in traction, but those are steeper and steeper in braking.

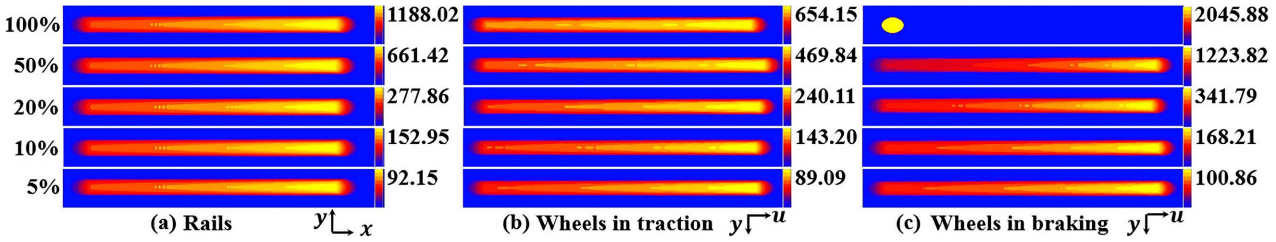

Figure 10. Temperature contours of the surface in the rolling direction at different slippages.

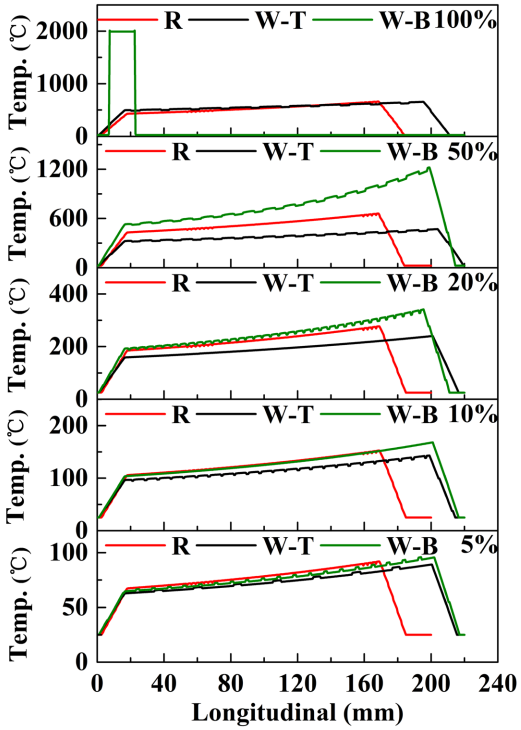

Figure 11. Temperature distributions in the rolling direction under at different slippages (R, W-T, W-B represent rail, wheel in traction and braking, respectively).

The vehicle speed directly affects the moving speed of the heat source. Whether in traction or braking, the temperature distribution in the rolling direction will be influenced by the speed. Figure 12 shows the temperature contours of the surface in the rolling direction at different speeds. With the increasing speed, the temperature contours are more and more uniform. Figure 13 is the temperature distribution of the nodes in the rolling direction, and the nodes are located in the line of rolling centers. At lower speeds, the temperature curves tend to increase with increasing rolling distance. As the speed increases, the temperature curves in the moving ranges of the heat source become flatter and flatter. The results indicate that the heat has no time to diffuse in a short period, which causes a high level of temperature around the contact area and will make a big difference in the adhe-

sion performance between the traction and braking.

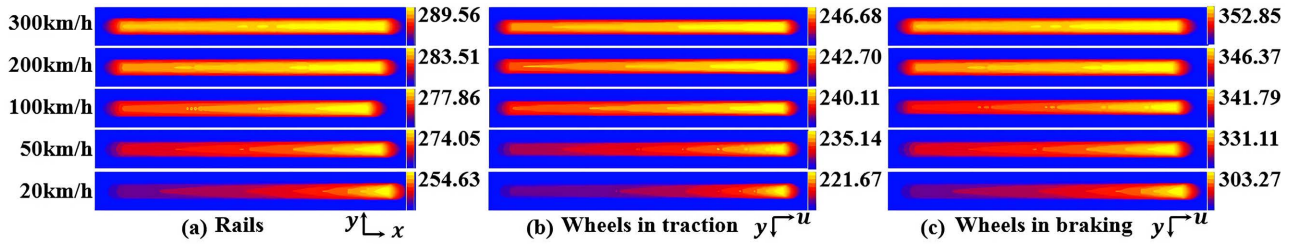

Figure 12. Temperature contours of the surface in the rolling direction at different speeds.

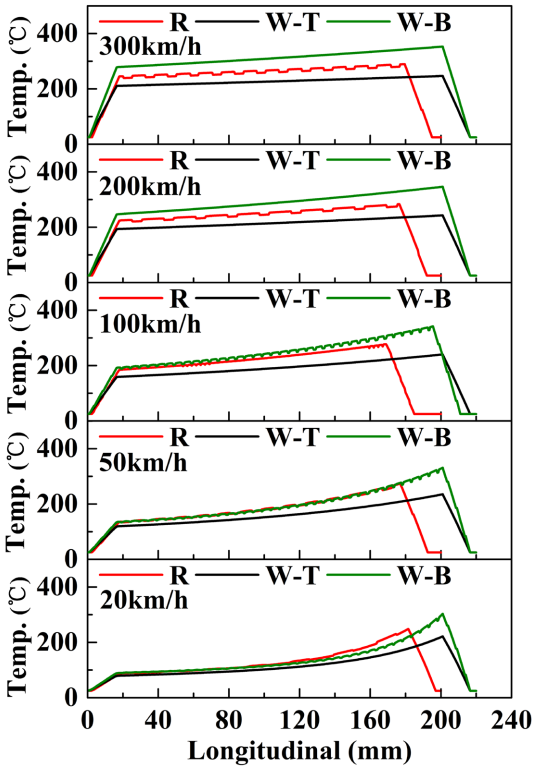

Figure 13. Temperature distributions in the rolling direction under at different speeds (R, W-T, W-B represent rail, wheel in traction and braking, respectively).

To reduce computational complexity, a constant friction coefficient was employed during modelling, meaning the coefficient remains unchanged with temperature variations. This approach is viable for comparing wheel-rail contact temperature rise during traction and braking states. However, it should be noted that this simplification introduces a degree of error into the calculation results. The next step in model optimisation involves adopting a temperature-dependent friction coefficient to enable the timely calculation and updating of heat flux values.

5. Conclusions

Based on the software MSC. Marc, a Fortran subroutine, was adopted to develop a 3D FE model for simulating wheel/rail contact temperature. The temperatures

under traction and braking were calculated, and the effects of slippage and speed on the temperature field were analyzed. The conclusions are as follows:

The wheel under braking gets the highest temperature, followed by the rail, and the wheel under traction gets the lowest temperature. When the slippage is less than 20%, the difference of the peak temperatures of the wheel under baking and traction is within 101.68˚C. After exceeding 20%, the difference increases sharply. The difference is not sensitive to vehicle speed, which keeps about 100˚C when the vehicle speed is over 50 km/h.

The largest drop rate of the temperature is the wheel in braking, followed by the rail, and the slowest one is the wheel in traction. The increase in the slippage expands this difference. At the same speed, the increasing rates of temperature are almost the same in traction and braking. However, as the speed increases, the temperature rises faster.

In the rolling direction, with the increasing slippage, the temperature distributions of the wheel in traction are more and more uniform, but the temperature difference between the leading and trailing edge under traction is larger and larger in braking. Under the extreme condition of the wheel sliding, the wheel temperature is concentrated on the contact patch. With the increasing speed, the temperature distributions of the wheel and rail are more and more uniform.

Funding

This research was supported by Guangzhou Railway Polytechnic Student Innovation and Entrepreneurship Projects (No. 2024CXCY008) and 2023 Guangzhou Railway Polytechnic Research Platform Project (No. GTXYP2302).

Conflicts of Interest

The author declares no conflicts of interest regarding the publication of this paper.

References

[1] Simon, I. (2006) Handbook of Railway Vehicle Dynamic. CRC/Taylor & Francis, 88-92.

[2] Tomberger, C., Dietmaier, P., Sextro, W. and Six, K. (2011) Friction in Wheel-Rail Contact: A Model Comprising Interfacial Fluids, Surface Roughness and Temperature. *Wear*, **271**, 2-12. https://doi.org/10.1016/j.wear.2010.10.025

[3] Pan, R., Ren, R., Chen, C. and Zhao, X. (2017) The Microstructure Analysis of White Etching Layer on Treads of Rails. *Engineering Failure Analysis*, **82**, 39-46. https://doi.org/10.1016/j.engfailanal.2017.06.018

[4] Kumar, A., Agarwal, G., Petrov, R., Goto, S., Sietsma, J. and Herbig, M. (2019) Microstructural Evolution of White and Brown Etching Layers in Pearlitic Rail Steels. *Acta Materialia*, **171**, 48-64. https://doi.org/10.1016/j.actamat.2019.04.012

[5] Chen, Y. and Lee, S. (2008) Elastic-Plastic Wheel-Rail Thermal Contact on Corrugated Rails during Wheel Braking. *Journal of Tribology*, **131**, Article ID: 011401. https://doi.org/10.1115/1.2991163

[6] Nakahara, T., Baek, K., Chen, H. and Ishida, M. (2011) Relationship between Surface Oxide Layer and Transient Traction Characteristics for Two Steel Rollers under Un-

lubricated and Water Lubricated Conditions. *Wear*, **271**, 25-31. https://doi.org/10.1016/j.wear.2010.10.030

[7] Zhu, Y., Olofsson, U. and Chen, H. (2013) Friction between Wheel and Rail: A Pin-On-Disc Study of Environmental Conditions and Iron Oxides. *Tribology Letters*, **52**, 327-339. https://doi.org/10.1007/s11249-013-0220-0

[8] Zhou, Y., Peng, J.F., Wang, W.J., Jin, X.S. and Zhu, M.H. (2016) Slippage Effect on Rolling Contact Wear and Damage Behavior of Pearlitic Steels. *Wear*, **362**, 78-86. https://doi.org/10.1016/j.wear.2016.05.001

[9] Popov, V.L., Psakhie, S.G., Shilko, E.V., Dmitriev, A.I., Knothe, K., Bucher, F. and Ertz, M. (2002) Friction Coefficient in "Rail-Wheel" Contacts as a Function of Material and Loading Parameters. *Physical Mesomechanics*, **3**, 17-24.

[10] Bucher, F., Dmitriev, A.I., Ertz, M., Knothe, K., Popov, V.L., Psakhie, S.G., *et al.* (2006) Multiscale Simulation of Dry Friction in Wheel/Rail Contact. *Wear*, **261**, 874-884. https://doi.org/10.1016/j.wear.2006.01.046

[11] Wei, Y., Wu, Y., Chen, K. and Sun, A. (2018) Experiment Research on Friction Coefficient between a Steel Plate and Rail in Transient Sliding Thermal Contact through a Pendulum. *Results in Physics*, **11**, 763-768. https://doi.org/10.1016/j.rinp.2018.10.025

[12] Carter, F.W. (1926) On the Action of a Locomotive Driving Wheel. *Proceedings of the Royal Society A—Mathematical Physical and Engineering Sciences*, **112**, 151-157.

[13] Tanvir, M.A. (1980) Temperature Rise Due to Slip between Wheel and Rail—An Analytical Solution for Hertzian Contact. *Wear*, **61**, 295-308. https://doi.org/10.1016/0043-1648(80)90293-8

[14] Knothe, K. and Liebelt, S. (1995) Determination of Temperatures for Sliding Contact with Applications for Wheel-Rail Systems. *Wear*, **189**, 91-99. https://doi.org/10.1016/0043-1648(95)06666-7

[15] Ertz, M. and Knothe, K. (2002) A Comparison of Analytical and Numerical Methods for the Calculation of Temperatures in Wheel/Rail Contact. *Wear*, **253**, 498-508. https://doi.org/10.1016/s0043-1648(02)00120-5

[16] Wu, L., Wen, Z., Li, W. and Jin, X. (2011) Thermo-Elastic-Plastic Finite Element Analysis of Wheel/Rail Sliding Contact. *Wear*, **271**, 437-443. https://doi.org/10.1016/j.wear.2010.10.034

[17] Asih, A.M.S., Ding, K. and Kapoor, A. (2012) Modelling Rail Wear Transition and Mechanism Due to Frictional Heating. *Wear*, **284**, 82-90. https://doi.org/10.1016/j.wear.2012.02.017

[18] Wu, Y., Wei, Y., Liu, Y., Duan, Z. and Wang, L. (2017) 3-D Analysis of Thermal-Mechanical Behavior of Wheel/Rail Sliding Contact Considering Temperature Characteristics of Materials. *Applied Thermal Engineering*, **115**, 455-462. https://doi.org/10.1016/j.applthermaleng.2016.12.136

[19] Naeimi, M., Li, S., Li, Z., Wu, J., Petrov, R.H., Sietsma, J., *et al.* (2018) Thermomechanical Analysis of the Wheel-Rail Contact Using a Coupled Modelling Procedure. *Tribology International*, **117**, 250-260. https://doi.org/10.1016/j.triboint.2017.09.010

[20] Yang, L., Hu, M., Zhao, D., Yang, J. and Zhou, X. (2020) Thermo-Mechanical Analysis of Train Wheel-Rail Contact Using a Novel Finite-Element Model. *Industrial Lubrication and Tribology*, **72**, 687-693. https://doi.org/10.1108/ilt-07-2019-0298

[21] Vo, K.D., Tieu, A.K., Zhu, H.T. and Kosasih, P.B. (2015) The Influence of High Temperature Due to High Adhesion Condition on Rail Damage. *Wear*, **330**, 571-580. https://doi.org/10.1016/j.wear.2015.01.059

[22] Lian, Q., Deng, G., Tieu, A.K., Li, H., Liu, Z., Wang, X., *et al.* (2020) Thermo-Mechanical Coupled Finite Element Analysis of Rolling Contact Fatigue and Wear Properties of a Rail Steel under Different Slip Ratios. *Tribology International*, **141**, Article ID: 105943. https://doi.org/10.1016/j.triboint.2019.105943

[23] Marshall, M.B., Lewis, R., Dwyer-Joyce, R.S., Olofsson, U. and Björklund, S. (2006) Experimental Characterization of Wheel-Rail Contact Patch Evolution. *Journal of Tribology*, **128**, 493-504. https://doi.org/10.1115/1.2197523

[24] Limpert, R. (1976) Engineering Design Handbook, Analysis and Design of Auto-Motive Brake Systems. US Army Material Development and Readiness Command, 28-29.

[25] Bergman, T.L., Lavine, A.S., Incropera, F.P. and Dewitt, D.P. (2011) Fundamentals of Heat and Mass Transfer. 7th Edition, John Wiley & Sons, Inc., 455-459.